Role of buoyant flame dynamics in wildfire spread

Mark A. Finney[a,1], Jack D. Cohen[a], Jason M. Forthofer[a], Sara S. McAllister[a], Michael J. Gollner[b], Daniel J. Gorham[b], Kozo Saito[c], Nelson K. Akafuah[c], Brittany A. Adam[c], and Justin D. English[c]

[a]Missoula Fire Sciences Laboratory, US Forest Service, Missoula, MT 59808; [b]Department of Fire Protection Engineering, University of Maryland, College Park, MD 20742-3031; and [c]Department of Mechanical Engineering, University of Kentucky, Lexington, KY 40506-0503

Edited by Robert E. Dickinson, The University of Texas, Austin, TX, and approved June 19, 2015 (received for review March 6, 2015)

Large wildfires of increasing frequency and severity threaten local populations and natural resources and contribute carbon emissions into the earth-climate system. Although wildfires have been researched and modeled for decades, no verifiable physical theory of spread is available to form the basis for the precise predictions needed to manage fires more effectively and reduce their environmental, economic, ecological, and climate impacts. Here, we report new experiments conducted at multiple scales that appear to reveal how wildfire spread derives from the tight coupling between flame dynamics induced by buoyancy and fine-particle response to convection. Convective cooling of the fine-sized fuel particles in wildland vegetation is observed to efficiently offset heating by thermal radiation until convective heating by contact with flames and hot gasses occurs. The structure and intermittency of flames that ignite fuel particles were found to correlate with instabilities induced by the strong buoyancy of the flame zone itself. Discovery that ignition in wildfires is critically dependent on nonsteady flame convection governed by buoyant and inertial interaction advances both theory and the physical basis for practical modeling.

wildfires | buoyant instability | flame spread | convective heating

Wildland fires are distinguished from industrial and urban fires by the kinds and sizes of the fuels available. Forests, shrublands, and grasslands are characterized by small, discrete particles, such as leaves, pine needles, grasses, bark, twigs, and other wood particles, which are highly dissected compared with pools of liquid fuel spills or the large, continuous, solid surfaces of furniture and buildings. All fires spread by transferring heat from the burning zone to new fuels (1), but the complex chemical nature of natural fuels (2), the fineness of the fuel particles in wildland fires and their separation by air spaces, create fire-spread conditions much different from those in urban fires. In fact, decades of research into ignition processes have not established an accepted theory explaining the ignition and spread of wildfires (3). Without a theory based on fundamental principles, the feedback processes of heat transfer and combustion that govern spread rates and the potential for extinction cannot be reliably modeled. Thus, fire-spread modeling has been based on widely varying physical assumptions (4) and empirical relationships applied to steady-state conditions. Although still useful, these approaches are inadequate for predicting fire spread in a variety of fuel complexes; estimating fire effects on vegetation, soils, and the atmosphere; training firefighters to recognize imminent hazards; and expanding opportunities for vegetation management. As wildfires increasingly impact human communities worldwide, climates continue to change, and more land is developed for human habitation and industry (5, 6), the need for a deeper understanding of wildland fire spread has become more urgent.

The study of physical processes associated with the spread of wildland fires began in the 1940s with the recognition that fuel particles ignite after sufficient amounts of radiative and convective heat are transferred to them from a burning zone (7). Many models have been based on this understanding, but consensus has not been reached on the respective roles of radiation and convection on fire spread (4). Radiation has been the most intensively studied and has often been assumed to govern spread (3), but recent findings reveal that the heat flux from radiation is insufficient alone to support fire spread. Individual fine particles will not ignite solely from radiation even at the preignition fluxes reported for forest crown fires (<~80 $kW{\cdot}m^{-2}$) (3, 8). The explanation is twofold: First, radiation is heavily attenuated in porous fuel beds, where vegetation blocks some fraction of radiation from the burning zone to unignited fuels until the fire is very near (9). In fire-spread experiments using shallow beds of dry fuels, particle temperatures rose sharply only when the leading edge of the fire was within centimeters of the particles (10, 11). Second, ignition of small particles by radiant fluxes found in wildland fires is "convection controlled" (12), meaning that the thin thermal boundary layer afforded by the short characteristic length scale confers efficient convective cooling by ambient air (13–15). Wildland fuel beds with typically fine-sized fuel particles (16) exhibit high convection heat transfer (3, 17) because heat transfer coefficients for free and forced convection are an inverse function of characteristic surface length, rising dramatically below 1 mm (3, 13). If radiation itself is insufficient to account for fire spread among small wildland fuel particles, convection must provide the explanation.

Here we focus on the role of convective heating in wildfire spread. Unfortunately, few studies have been conducted on convective heating of fine fuels in wildland fires or the flame dynamics that produce and transport convective heat. If convection is modeled at all, turbulent diffusion is assumed (18). It is known, although, that flames in spreading fires can exhibit periodic behavior (19) and intermittently sweep or burst forward to heat and ignite fuel particles (20–23), but these reports provide little insight into the origins or structure of these flame bursts or consequences for particle ignition. Here we report previously

Significance

Wildfires burn millions of hectares per year on every inhabited continent, but the physical mechanism governing spread is not known. Models of wildfire spread are widely used for prediction, firefighter training, and ecological research but have assumed various formulations of known heat transfer processes (radiation and convection) absent a definitive theory of their organization. New experimental evidence reported here reveals how buoyancy generated by the fire induces vorticity and instabilities in the flame zone that control the convective heating needed to ignite fuel particles and produce spread.

Author contributions: M.A.F., J.D.C., J.M.F., and M.J.G. designed research; M.A.F., J.D.C., J.M.F., S.S.M., M.J.G., D.J.G., B.A.A., and J.D.E. performed research; M.A.F., J.D.C., S.S.M., M.J.G., D.J.G., K.S., N.K.A., and J.D.E. contributed new reagents/analytic tools; M.A.F., J.D.C., M.J.G., D.J.G., K.S., N.K.A., B.A.A., and J.D.E. analyzed data; and M.A.F., J.D.C., M.J.G., K.S., and N.K.A. wrote the paper.

The authors declare no conflict of interest.

This article is a PNAS Direct Submission.

Freely available online through the PNAS open access option.

[1]To whom correspondence should be addressed. Email: mfinney@fs.fed.us.

This article contains supporting information online at www.pnas.org/lookup/suppl/doi:10.1073/pnas.1504498112/-/DCSupplemental.

overlooked explanations for forward bursts of flame and describe the similarity of flame behaviors to buoyancy-inertia–driven instabilities observed in other fields of fluid dynamics. We demonstrate how these dynamics force flames downward and forward into fuel beds, appearing to play a central role in organizing the convective heat transfer needed for wildfire spread. Intermittency of convective heating is then explored in terms of frequency scaling and its consequences to fuel particle ignition.

Explaining Flame Structure

Saw-toothed flame geometry (20) was observed repeatedly in laboratory-scale and field-scale fires, both stationary and spreading. This flame geometry was followed by stream-wise streaks of smoke and flames behind the flame zone (Fig. 1). High-speed imaging of flame and smoke movements revealed that counter-rotating vortex pairs force flames downward into troughs and upward into peaks (Movies S1–S3). This flame geometry and its underlying vorticity (Fig. 2) strongly resemble the circulations arising from centrifugal instability of horizontal flows lifted by concave surfaces (24–26) and from buoyant flows along heated plates (27, 28). In laboratory studies, these are known as counter-rotating Taylor-Görtler vortex pairs (24, 26) that are oriented parallel to the flow direction. They produce alternating upward and downward flows at their convergence zones in regular repetition (29) (Fig. 2). In field-scale fires, evidence of similar flow instability and vorticity has been reported as flame "towers and troughs"; these were recorded through infrared videography of an approaching experimental Canadian crown fire (30) and Australian grass fire (31).

Regularly spaced streaks behind the flame front correspond to smoldering combustion (Fig. 1*E*) beneath flame peaks. These were visualized as isosurfaces of helicity in the vicinity of the fireline during numerical simulations of wildfire spread (32) (Figs. 1*G* and 2). These stream-wise vortices are not to be confused with shear-induced horizontal rotations at the outer edges of rising thermal plumes (33), which are elevated above the fuels. Instead, the vortex pairs described here force flames and hot gases downward and forward, splaying them horizontally within the fuel bed (Figs. 2 and 3). At the leading edge of the fire, these vortices force hot gases down onto fuel particles ahead of the fire (Movies S3–S6). In both laboratory- and field-scale fires, the average separation between these vortex pairs (flame front peaks and troughs) scaled linearly with flame length (Fig. 1*I*). This relationship raises significant questions about the origins of the stream-wise vorticity and the possibility that vortex spacing correlates with boundary-layer thickness, which similarly increases with scale (25, 34).

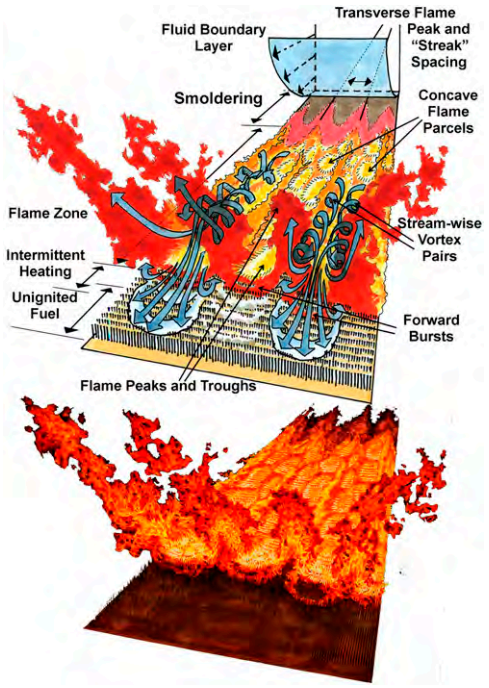

Fig. 2. Illustrations of flame dynamics and related flow instabilities observed in experimental burns. Flame-zone buoyancy creates stream-wise vortex pairs that alternately push flames up into peaks and down into troughs. Streaks of smoldering combustion aligned with flame peaks extend back behind the front. Concave flame parcels travel through the flame zone and burst intermittently forward through the troughs to heat unignited fuels.

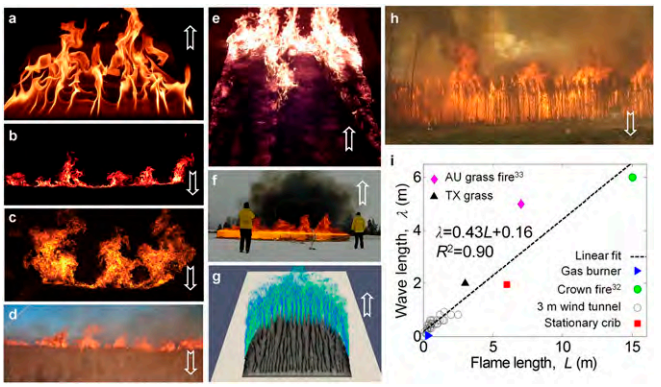

Fig. 1. Images of saw-tooth geometry and stream-wise streaks in flame fronts at laboratory and field scales. Arrows indicate wind or spread direction. (*A*) Top view of stationary flames from an ethylene gas burner. (*B*) Laboratory fire with 0.40-m flames (*C*) Same as in *B* but with 1.5-m flames. (*D*) Front view of 3-m-tall flames from an approaching heading fire in Texas grassland. (*E*) Top view of burn streaks behind flame zone. (*F*) Stationary fire with 6-m flames on 16-m wooden crib. (*G*) Numerical simulation of wildfire with an ~6-m flame length (reprinted from ref. 32, with permission from Elsevier; www.sciencedirect.com/science/journal/01681923). (*H*) Front view of experimental crown fire in Canada with an ~15-m flame length (image courtesy of the US Department of Agriculture, Forest Service; related to crown fires in ref. 30). (*I*) Plot of separation between flame peaks (same as stream-wise streak spacing) in relation to flame length.

Scaling of Flame Intermittency

Characterizing convective heating within flames is complex because flames are highly nonsteady. For example, temperatures recorded at the edge of spreading and stationary fires fluctuated from nearly ambient to over 1,000 °C multiple times per second (Fig. 4). We used high-speed videography to associate these flame-burst signals with the passage of coherent motions through the flame zone. Although the precise source(s) of these motions are not fully understood, their behavior over scales of several magnitudes and subsequent effects on wildland fire spread are described below.

Coherent motions were observed in overhead videos (Movie S1) as span-wise wrinkles originating near the trailing edge of flame zones (Figs. 2, 3 *A* and *B*, and 4*A*). A sequence of these wrinkles defines a coherent concave parcel (Fig. 4*A*) that is advected forward to exit ahead of the fire as a flame burst (Fig. 2, Fig. 3 *D* and *E*, and Movies S2, S4, and S5). The repetition of bursts causes intermittent flame impingement on fresh fuel particles. At the leading flame edge we also observed transverse motion: flame peak and trough structures moved sideways, back and forth along flame fronts. Sinuous, lateral meandering of vortex boundaries has similarly been noted for Taylor-Görtler vortices when the boundary layer becomes turbulent; such meandering patterns are also periodic in time (26, 35, 36). Both

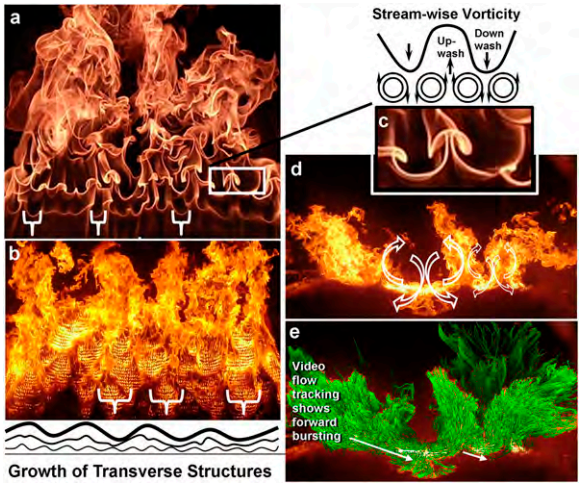

Fig. 3. Images from behind the flame zone illustrate buoyant instabilities forming as transverse waves (brackets) that advect forward in (*A*) a stationary ethylene gas burner and (*B*) a wind-tunnel experimental fire spreading in cardboard fuel (Movie S1). Stream-wise (longitudinal) vortices (*C*) induce flame peaks and troughs at up-wash and down-wash convergence zones. Movie images (Movies S2 and S4) at the leading edge of spreading fires (*D*) show flame vortex circulations and forward flame bursts through flame troughs after flow-tracking analysis (*E*).

longitudinal motion (stream-wise) and transverse motion may contribute to the fluctuating temperature patterns (Fig. 4 *B–D*), but transverse waves appear responsible for the flame bursts that occur ahead of the forward edge of the flame zone. Both structures provide coherency to flame motions as they penetrate the fuel bed, which is evident not only in movies of stationary flames but also in temperatures recorded by a stream-wise linear array of thermocouples in spreading laboratory and field-scale fires (Fig. 4 *C* and *D*).

We found that coherent flame motions produced intermittent temperature fluctuations with predictable average frequencies. These frequencies introduce intermittent thermal boundary conditions on fine fuel particles that affect their ignition response (37) and may yield insights into buoyant dynamics and eventual modeling of the reacting flow field. Time-averaged frequencies of "bursting events" in turbulent boundary layers are obtained by counting the irregular excursions of temporal variance in flow velocity (38–40). In similar fashion we quantified average flame burst frequencies using thermocouple readings at the leading edge of spreading fires and high-speed movies of stationary fires. For all flame sources we calculated a variable interval, time-averaged (VITA) frequency, f, and expressed it as a correlation between the Strouhal number ($fL\ U^{-1}$) and Froude number $[U^2\ (gL)^{-1}]$, defined in a manner similar to the description of puffing in pool fires (41–43), except scaled with flame length L and wind speed U (Fig. 4*E*). The flame length was chosen as the characteristic length scale as it best represented the fire size or intensity of spreading line fires ($kW{\cdot}m^{-1}$) (44) or stationary burners (kW/m^{-2}) (45). Other variables such as horizontal flame zone depth yielded no correlation. The exponent of −0.40 of this correlation is close to the −0.5 exponent for diameter scaling of the puffing frequency in circular pool fires (41–43). In pool fires, this relationship implies that puffing frequency increased with fuel flow velocity but decreased with pool diameter. The same correlation has been proposed in nonfire buoyant releases (e.g., helium) from circular (46) and rectangular sources (47). For our fires where the wind and buoyancy are in perpendicular directions (vs. the parallel fuel flow and buoyancy for pool fires), frequency increased with wind speed but decreased with flame length. The correlation and exponent changed little whether flame length was taken from ocular estimates or calculated from energy release rate with formulas for our spreading fires (44) or stationary fires (45). The robustness of such correlations across many orders of magnitude in Froude number suggests that buoyancy and flow-related instabilities in free-burning fires are weakly dependent upon the fuel source (43, 48). The flame structure and flame burst frequency in this study were consistent from laboratory to field scales because of the narrow temperature range (900–1,200 °C) and thus relatively consistent gas densities (buoyancy) within nonpremixed flames in these free-burning fires (45, 48).

Our field-scale data from spreading fires in Texas grasslands (Fig. 4*C*) and the large-scale outdoor stationary crib fires (Fig. 4*D*) agreed with this scaling (Fig. 4*E*). Scatter in the correlation may be related to the variability of the scaling variables, which are mean values of wind speed and flame length. Our ability to extend and confirm this scaling with data from large-scale wildfires is limited because frequency data are rarely measured in the field. In one known case, a prescribed crown fire in Alaska, the observed flame burst frequency was 0.555 Hz (49), which is in accord with our experimental data (Fig. 4*E*). Furthermore, descriptions of vorticity and repeated forward bursting of flame troughs at the front of an experimental Canadian crown fire (30) accurately applied to our observations of laboratory fires. The strong scaling exhibited between the Froude number and forward flame bursts suggests a possible explanation for why scaling analysis of convective heating in surface fires (50) could be successfully applied to crown fires (51).

Convective Heating and Fuel Particle Ignition

Effects of flame radiation and intermittent convection from flame bursts on particle heating were studied in spreading laboratory fires using a water-cooled radiometer and thermocouples to measure both air and fuel particle surface temperature. As the flame front approached, the surface temperature of fine 1-mm diameter particles (Fig. 5*A*) increased slowly by radiation (~5 °C·s^{-1}) but always remained below ~100 °C. When contacted intermittently by bursts of flame and hot gasses ahead of

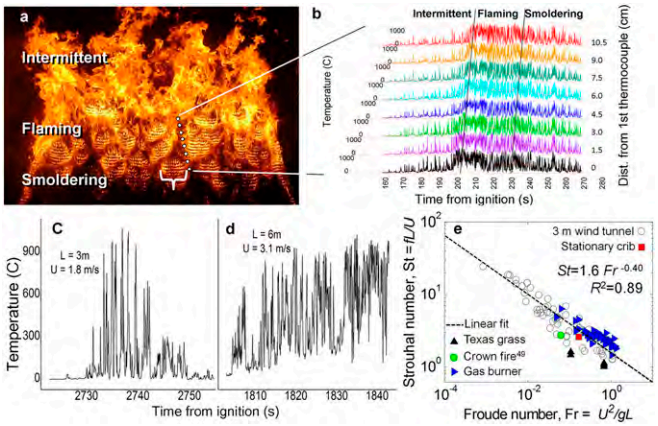

Fig. 4. Overhead view of a laboratory fire spreading away from camera through a cardboard fuel bed shows (*A*) coherent parcels of flame surface (bracket) generated by transverse instabilities in the flame zone and approximate locations of thermocouples, which (*B*) record temperature fluctuations before ignition when coherent flame structures burst forward within the intermittent flame zone of the fuel bed (spline curves distinguish flaming to intermittent transition). Temperature fluctuations recorded by thermocouples in spreading grass fires (*C*) and a stationary crib burn (*D*) were plotted with time-average frequency of flame intermittency from all sources (*E*) to reveal a strong relationship between Strouhal number ($St = fL\ U^{-1}$) and Froude number $[Fr = U^2\ (gL)^{-1}]$ scaled by wind speed U and flame length L.

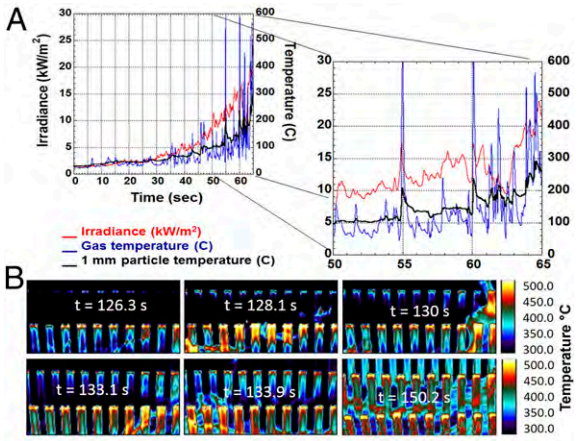

Fig. 5. Time series of irradiance, air temperature, and 1-mm particle surface temperature during flame spread in cardboard fuel bed (*A*). Fine particles heat and cool rapidly as intermittent flame contacts produce a stair-step temperature rise to ignition. Radiation preheating indicated when particle surface is warmer than air. Thermal infrared image sequence (*B*) from above and behind the fire show heating patterns on rows of 6-mm-wide cardboard particles as fire approaches. Higher temperature and ignition of corners and edges indicate convection as the principal heating mechanism.

the fire front (indicated by spikes in air temperature), the particle temperature increased and decreased rapidly (~2,500 °C·s^{-1}). The intermittency resulted in a stair-step heating of the fine particles until ignition. Coarser particles showed a similar stair-step heating pattern with significantly lower thermal response rates (~100 °C·s^{-1}) and remained below the nominal ignition temperature of cellulosic materials (~350 °C) until flame contact was continuous (surrounding fuels were ignited). Infrared thermographic images of cardboard particles (6 mm wide) in spreading laboratory fires showed higher temperatures at their corners and edges than on their flat faces (Fig. 5*B*). This heating pattern is consistent with thinner boundary layers at the short length scales of corners and edges and thus increased convective heating from hot flow over cooler surfaces, confirming an important role of convective heating in the ignition of particles of varying sizes.

The radiation heat fluxes measured during the laboratory-scale fires were generally below ~30 kW·m^{-2} during preheating with infrequent higher irradiances for durations less than 4 s. Experiments have shown (3, 52) that this level of radiation requires exposure of fuel particles longer than the total 2- to 35-s flame residence times produced in the wind tunnel experiments. Although previous laboratory-scale fire studies (9–11, 53) have failed to resolve the heat transfer mechanisms when flame fronts were within 5 cm and fuel particles heated to ignition, our data clearly link intermittent flame and hot gas contact generated by instabilities to fine particle heating, which is sensitive to the frequency of intermittent thermal boundary conditions (37). This repetitive convective heating thus appears to be the critical heat transfer mechanism causing ignition and spread of these fires.

Understanding How Wildfires Spread

Our experiments have suggested a significant, missing physical component of wildfire spread and highlight the challenges facing numerical modeling and future research. Fine-particle ignition in spreading fires appears to be tightly coupled to forward convection from buoyancy-inertia–induced flame bursts at timescales of 10^{-1} s and length scales of 10^{-2} m. The Strouhal number–Froude number relationship suggests that this forward convective heat transfer becomes more intermittent with greater buoyancy (longer flames), but the heating distance may diminish with steeper flame trajectory at lower Froude numbers (54). High-fidelity numerical models can potentially represent such processes for research at laboratory scales, but models intended for the large domains of actual wildfires (32, 55) must use coarser resolutions and parameterize the convective heat transfer and ignition processes based on careful comparison with experimental data. This initial work on scaling the intermittency of heating is a first step not only in understanding the physical process, but also in parameterizing heating in a way useful for future modeling efforts. Research will be needed to help understand the sensitivity to vorticity generation and initial conditions of fluid instabilities that grow downstream into the observed flame structures. Our findings will likely require a new examination as to how familiar biophysical factors, such as topography, heterogeneous fuel patterns, moisture of dead and live vegetation, and atmospheric dynamics at larger scales, influence buoyant processes that we observe to govern particle heating and wildfire spread. Both field and laboratory data can help examine these and related questions, particularly the extension and limits of scaling relations over a wider range of wildfires in different weather and fuel conditions. For example, does fire spread in fuel types composed of large particles (logs, logging debris) occur primarily by radiation as suggested by the physics of particle heat exchange? Such research will ultimately lead to discovering how wildland fuel properties (amounts, distributions, etc.) affect fire behavior and thereby improve techniques for characterizing vegetation, assessing spread potential, and mitigating fuel hazards. Although integration of these concepts into practical models will require additional work, our findings have begun to penetrate some of fire's long-held mysteries and outline a theory of wildfire spread.

Materials and Methods

Flame structure and particle ignition were studied using laboratory-scale fires at the wind tunnel facility of the Missoula Fire Sciences Laboratory (MFSL) and the University of Maryland (UMD), and field-scale fires at the MFSL and Fort Swift, Texas. The MFSL has a 3- × 3-m cross-section wind tunnel in which stationary and spreading fires were studied. UMD has a 0.3- × 0.3-m cross-section wind tunnel used to study stationary flame sources from gas burners and fuel-soaked wicks.

Spreading Fire Experiments. Fire spread experiments at the MFSL used uniform fuel beds 1.22–2.45 m in width and 6 m in length made of laser-cut cardboard. This new technique controls for precise physical dimensions of particles (length, surface area) and arrangement (position, separation). A commercial CO_2 laser system was used to cut cardboard fuel elements at regular parallel spacing attached to a common spine, resembling a "comb." The cardboard, known as brown "chip board," was 1.27 mm (0.05 inch) thick with ~60% recycled content and a mass density of 600 kg·m^{-3}.

These fuel beds were burned in the MFSL wind tunnel. The wind profiles are laminar except along the bottom surface where an upstream trip fence produces a turbulent boundary layer ~0.25 m thick at the start of the fuel bed. Wind speeds were varied from 0.22 to 2.3 m·s^{-1} with relative humidity of ~25%. The combs were supported and arranged on a foundation of cement-board strips 0.635 × 5.08 cm each, separated by a steel spacer 0.158 × 2.54 cm that exposed only the vertical tines. Tine lengths of 2.54, 10.1, 20.3, and 35.6 cm were used in the burns. The longitudinal spacing of the combs could be adjusted every 0.64 cm, allowing control of exact fuel bed properties including packing ratios (0.00133–0.088) and loading (0.079–2.682 kg·m^{-2}). Range of flame length in experimental burns varied from 0.1 to 2.5 m and spread rate varied from 0.57 to 7.72 m·min^{-1} (Table S1). To limit lateral air entrainment causing flame front curvature, the sides of the beds were lined with paper treated with the flame retardant $(NH_4)_2HPO_4$ to limit independent flaming combustion but allow the paper to burn in conjunction with the advancing fire front (21). The consumption of the paper sideliners at the trailing edge of the burning zone avoids channeling of air inflow to the rear of the fire, which has been shown to affect fire spread on slopes (19).

Temperature fluctuations at the upper surface of the fuel bed were measured with a linear rake of 64 thermocouples (Type K, bead thickness 0.025 mm) oriented in the stream-wise direction. The first 32 thermocouples

were spaced 1.5 cm apart, and the second 32 thermocouples were spaced 3.0 cm apart. The thermocouple beads were positioned vertically at the top of the fuel and laterally 0.7 m inside the fuel bed, as measured from the lateral edge. Data were recorded at 500 Hz with a National Instruments Inc. data acquisition system. Digital video cameras recording at 60 frames per second were positioned at upwind, downwind, overhead, lateral, and oblique angles to capture flame structure and dynamics. High-speed movies taken at 300 frames per second were used to record flame impingement on fuel particles at the leading edge of some of the burns. Movie segments were processed using flow-tracking analysis software (60) to visualize flame parcel movement related to vorticity and bursting (Fig. 3*E* and Movie S2).

Gas Burner Experiments. Stationary forced-flow experiments were performed at the MFSL and UMD. At the MFSL, a propane burner used sintered metal as the porous burner surface measuring 0.3 by 0.25 m. A volumetric flow meter controlled the flow rate of propane gas to achieve energy release rates of 7.5, 10.9, and 15.1 kW. Ceramic insulation board surrounding the burner made a continuous flat surface that limited side-air entrainment. The apparatus was tested at free-stream velocities of 0.22, 0.44, 0.67, 0.89, 1.11, and 1.34 $m{\cdot}s^{-1}$. Side view video was captured with a Phantom brand high-speed camera at 120 frames per second.

At UMD, a laminar wind blower was designed and built for uniform forced-flow combustion experiments. The wind blower pressurized a 0.75-m^3 plenum box with a centrifugal fan, producing a fully developed laminar boundary layer exhausted at the duct outlet 1.35 m downstream. The velocity profile of the boundary layer was measured along the center line of the blower above the burner surface using a hot-wire anemometer and confirmed precise forced-flow control between 0.6 and 4.8 $m{\cdot}s^{-1}$ with turbulence intensities less than 3% at maximum velocities. High-speed videography captured digital images of side and top views of the flame. The side-view camera was a Phantom, recording 120 frames per second at 1,920 × 1,080 pixel resolution. The top-view camera (Casio EFX-1, recording 120 frames per second at 640 × 480 resolution) was positioned directly above the rear burner edge and aimed forward to observe the flame leading edge at approximately a 45° angle.

Field Experiments. A wooden crib of rough-sawn 2.5-cm square ponderosa pine lath was burned to generate large-scale flame dynamics from a stationary source (Fig. 1*F*). The laths were arranged with square spacing (0.124 × 0.124 m) stapled at the ends with the intent of achieving non-ventilation limited burning. Cribs were 1.2 m wide and 0.61 m tall and constructed in 2.4-m-long sections that were assembled in the field to create an overall length of 15.8 m (Fig. 1*F*). The crib was arranged in a normal orientation to the prevailing wind direction and burned on January 30, 2014, in an outdoor field 250 m square with average wind speed of 3.1 $m{\cdot}s^{-1}$ measured by four cup-anemometers positioned at 6.1 m height. Flames extended from the bed ∼6 m and deflected downwind. Four thermocouple rakes, each with a linear series of 16 fine-wire 0.025-mm thermocouples spaced 0.2 m apart and 1 m above ground, were located in a normal orientation to the crib in the downwind direction to record temperature fluctuations with a Campbell Scientific CR1000 data logger at 33.33 Hz. Flame structure was documented with digital movie cameras surrounding the crib recording at 60 frames per second. Vertical scale was referenced visually from poles with 0.25-m graduations.

Five grass plots (5 ha each) were burned at Camp Swift, Texas, on January 15, 2014. Average wind speeds during ∼3 min of burning on each plot were calculated as 1.8 $m{\cdot}s^{-1}$ for the first three plots and 4.5 $m{\cdot}s^{-1}$ for the final two plots using anemometer recordings (3-s intervals) located at the plot corners. Dry fully cured grass was ∼1 m tall and produced flames ∼3 m high. Before ignition, two thermocouple rakes were positioned 1 m above the ground surface (top of the grass) and oriented perpendicularly to the prevailing wind. Plots were ignited along the upwind edge with a drip torch to generate a linear heading fire (spreading with the wind) into the instrumentation site. Each rake supported 32 Type K 0.025-mm fine-wire thermocouples spaced at 0.2 m with temperature recorded by a Campbell Scientific CR1000 data logger at 33.33 Hz. Movie cameras recording at 60 frames per second were located at fixed positions around the plots from multiple angles to capture flame structure and dimensions.

Analysis. Movies for laboratory and field burns were studied to obtain visual estimates of flame length and spacing between flame peaks. Flame length was visually estimated relative to measured reference points in the laboratory and field. For laboratory burns, visual estimates were corroborated against flame length transformed from fireline intensity (44) ($kW{\cdot}m^{-1}$) ($y = 1.0954\times - 0.5218$, $R^2 = 86\%$), which is the product of measured spread rate, fuel loading ($kg{\cdot}m^{-2}$) consumed in flaming, and heat content of gaseous combustion (56) ($14\ MJ{\cdot}kg^{-1}$). Most cardboard fuel mass was consumed in the flaming phase, and the preburn loading was used for these calculations. Spacing between peaks from spreading fires was calculated by counting the flame peaks in movie frames and dividing by the known width of experimental fuel beds and the reference distances in Texas grass burns.

Temperature fluctuations in MFSL spreading fires were clearly visible in the temperature time-series data recorded by the thermocouple arrays (Fig. 4), as were bursts of the flame beyond the mean flame front in stationary burners. The variable of primary interest for the spreading laboratory fires was the flame burst frequency before ignition because these signals reflect conditions influencing particle heating. Preignition was defined from the first crossing of the 350 °C temperature to where a spline smoothing of the temperature data reached its peak (Fig. 4*B*). The 350 °C temperature represents a useful but approximate surface temperature at pilot ignition of wood fuel (57) although sustained flaming ignition actually depends upon a critical mass flux (3). The average temperature frequency for the preignition period was obtained using the level crossing of temperature spikes above 350 °C that equates to the VITA method applied to determine frequency of turbulent bursts in boundary layer flows (40). Fourier analysis is difficult to apply because of nonperiodic "spikey" temperature fluctuations (not sinusoidal). The same VITA method was applied to temperature data taken from the Fort Swift grass burns. Analysis of the crib burn omitted the spline fit because it was a stationary flame source.

Nonsteadiness of downstream flame locations was studied in stationary gas burner experiments using side-view high-speed movies and an array of thermocouples ahead of the burner. Image frames were converted to binary (flame, no-flame), and the frequency of the flame pulsations was determined using the VITA method (40) at a range of locations starting at the burner edge and increasing in 1-cm increments. The flame position in time was compared with each of these locations and the number of occurrences was tallied. The frequency at each location was determined as the number of crossings in the total number of frames multiplied by the frame rate of the movie. The maximum VITA frequency among all downstream locations was used for scaling comparison with spreading fire data.

Scaling Laws and Scaling Analysis. We examined the application of scaling laws developed for stationary pool and crib fires (58) and for spreading fires (59) to the scaling of our flame intermittency measurements. Of the six different pi numbers in these laws, the Froude number (*Fr*) = (the inertia force of air)/(the buoyancy force acting on the heated gas and flame) relates to fluid motion, and the other five are related to the condensed and gas-phase heat balances. The dynamic aspect of flame in relation to the spread of wildfires may be addressed as a possible seventh pi number, π_7 = (dynamic force)/(the inertia force of horizontal flow). The denominator of π_7 is the same as the numerator of *Fr*, meaning that three different forces are assumed to control flame dynamics (the buoyancy force acting on the heated gas and flame, the inertia force of horizontal flow, and the dynamic force due to turbulent instability or buoyancy-driven instability or possibly coupling of both).

As the first step of investigating the appropriateness of π_7 for wildfire spread, we assumed that π_7 is the Strouhal number (*St*) and evaluated the Strouhal number ($fL\ U^{-1}$) and Froude number [$U^2\ (gL)^{-1}$] (*St–Fr*) correlation common to the study of pulsating pool fires (41, 43, 58). A high *St–Fr* correlation strengthens the interpretation of dynamic scaling in wildfire spread for the range of our scale model and outdoor experiments. Thus, $St = f\ LU^{-1}$ and $Fr = U^2(gL)^{-1}$ were obtained for flame intermittency measurements where *f* is the VITA frequency measured, *U* is the free-stream wind velocity, and *g* is acceleration due to gravity. Flame length was chosen as the characteristic length scale *L* and represents the magnitude of the buoyant force related to energy release rate in spreading fires (44) ($kW{\cdot}\ m^{-1}$) and non-spreading fires (45) ($kW{\cdot}m^{-2}$) and is practically useful as a visual indicator of wildfire intensity. Burner diameter has most often been used as the length scale for *St–Fr* scaling of pool fires (43), but the horizontal flame zone depth of our spreading and stationary fires did not yield significant correlation.

Particle Heating in Laboratory Fires. We measured fuel particle temperatures and adjacent convective temperatures and irradiances (Fig. 4) during fire-spread experiments in the MFSL wind tunnel facility. Fuel particles of two sizes (1- and 12-mm square cross-sections) were made of yellow poplar, placed end-to-end at the center and laterally across the top of experimental fuel beds and instrumented with a pair of fine thermocouples (0.051-mm diameter). One thermocouple was embedded in the center of the upwind particle surface and the other was located 5 mm away from the surface to measure air or flame temperatures. Rates of particle heating and cooling ($°C{\cdot}s^{-1}$) associated with intermittent flame pulses were calculated from thermocouple measurements

during the final 2 s before ignition. A water-cooled radiometer was placed at the level of the instrumented fuel particles and equidistant (65 mm) from each front-face embedded thermocouple. The 1-mm fuel particle is at the coarse limit of wildland fine fuels in the 1-h time-lag category based on characteristic surface area to volume ratios used in the United States (16).

Infrared thermography was used to capture the transient temperature history of 6.0-mm wide cardboard fuel particles approached by an advancing flame front (Fig. 5*B*). The FLIR SC4000 infrared camera has a spatial resolution of 320 × 256 pixels and a spectral range of 3–5 μm. A broadband flame filter with a spectral range of 3.7–4.2 μm allowed imaging of fuel-particle surface temperatures through the flame zone. The IR camera was fixed ~93 cm behind the spreading flame zone, looking down at the fuel bed with a view angle of 30.6° from the horizontal. The camera was housed in an air-purged aluminum container 33.02 cm in diameter containing ice packs to limit heating of the camera during burns. The amount of noise and saturation captured in each movie image was reduced using a superframing algorithm that repeatedly takes a succession of four images (subframes) at progressively shorter exposure times. The subframes from each cycle are merged into a single superframe to record thermal features across the temperature range.

ACKNOWLEDGMENTS. We thank Mark Vosburgh, Randy Pryhorocki, Andrew Gorris, Jay Fronden, Isaac Grenfell, Ian Grob, Dan Jimenez, Cyle Wold, Jane Kapler Smith, Raquel Hakes, and Ajay Singh for their assistance. Funding was provided by the US Forest Service Research and the National Fire Decision Support Center.

1. Drysdale D (1998) *An Introduction to Fire Dynamics* (John Wiley & Sons, New York), 2nd Ed, , Chap 7.
2. Sullivan AL, Ball R (2012) Thermal decomposition and combustion chemistry of cellulosic biomass. *Atmos Environ* 47:133–141.
3. Finney MA, Cohen JD, McAllister SS, Jolly WM (2013) On the need for a theory of wildland fire spread. *Int J Wildland Fire* 22(1):25–36.
4. Sullivan AL (2009) Wildland surface fire spread modeling, 1990–2007. 1. Physical and quasi-physical models. *Int J Wildland Fire* 18(4):349–368.
5. Marlon JR, et al. (2008) Climate and human influences on global biomass burning over the past two millennia. *Nat Geosci* 1:697–702.
6. Pechony O, Shindell DT (2010) Driving forces of global wildfires over the past millennium and the forthcoming century. *Proc Natl Acad Sci USA* 107(45):19167–19170.
7. Fons WL (1946) Analysis of fire spread in light forest fuels. *J Agric Res* 72(3):93–121.
8. Frankman DA, et al. (2013) Measurements of convective and radiative heating in wildland fires. *Int J Wildland Fire* 22:157–167.
9. Baines PG (1990) Physical mechanisms for the propagation of surface fires. *Math Comput Model* 13(12):83–94.
10. Fang JB, Steward FR (1969) Flame spread through randomly packed fuel particles. *Combust Flame* 13(4):392–398.
11. Rothermel RC, Anderson HE (1966) Fire spread characteristics determined in the laboratory. US Forest Service Research Paper INT-30. 34 pp.
12. Martin S (1965) Diffusion-controlled ignition of cellulosic materials by intense radiant energy. *Symp (Intl) Comb* 10(1):877–896.
13. Incopera FP, DeWitt DP (2002) *Fundamentals of Heat Transfer and Mass Transfer* (John Wiley & Sons, New York), 5th Ed, , Chap 9.
14. Alvares NJ, Blackshear PL, Kanury AM (1970) The influence of free convection on the ignition of vertical cellulosic panels by thermal radiation. *Comb Sci Tech* 1:407–413.
15. Garg DR, Steward FR (1971) Pilot ignition of cellulosic materials containing high void spaces. *Combust Flame* 17(3):287–294.
16. Scott JH, Burgan RE (2005) Standard fire behavior fuel models: A comprehensive set for use with Rothermel's surface fire spread model. *USDA For Serv* RMRS- GTR-153, 72 pp.
17. Tibbals EC, Carr EK, Gates DM, Kreith F (1964) Radiation and convection in conifers. *Am J Bot* 51(5):529–538.
18. Weber RO (1991) Modelling fire spread through fuel beds. *Prog En Comb Sci* 17(1): 67–82.
19. Atkinson G, Drysdale D, Wu Y (1996) Fire driven flow in an inclined trench. *Fire Saf J* 25(2):141–158.
20. Beer T (1991) The interaction of wind and fire. *Boundary-Layer Meteorol* 54(3): 287–308.
21. Byram GM, Clements HB, Elliott ER, George PM (1964) An experimental study of model fires. USDA Forest Service, *Southeastern Forest Experiment Station, Southern Forest Fire Laboratory*, Technical Report No. 3. (Macon, GA).
22. Morandini F, Silvani X (2010) Experimental investigation of the physical mechanisms governing the spread of wildfires. *Int J Wildland Fire* 19:570–582.
23. Dupuy JL, Marechal J, Portier D, Valette J-C (2011) The effects of slope and fuel bed width on laboratory fire behavior. *Int J Wildland Fire* 20(2):272–288.
24. Meroney RN, Bradshaw P (1975) Turbulent boundary-layer growth over a longitudinally curved surface. *AIAA J* 13(11):1448–1453.
25. Hoffmann PH, Muck KC, Bradshaw P (1985) The effect of concave surface curvature on turbulent boundary layers. *J Fluid Mech* 161:371–403.
26. Saric WS (1994) Görtler vortices. *Annu Rev Fluid Mech* 26:379–409.
27. Sparrow E, Husar R (1969) Longitudinal vortices in natural convection flow on inclined plates. *J Fluid Mech* 37(2):251–255.
28. Jeschke P, Beer H (2001) Longitudinal vortices in a laminar natural convection boundary layer flow on an inclined flat plate and their influence on heat transfer. *J Fluid Mech* 432:313–339.
29. Maughan J, Incropera F (1987) Secondary flow in horizontal channels heated from below. *Exp Fluids* 5(5):334–343.
30. Clark TL, Radke L, Coen J, Middleton D (1999) Analysis of small-scale convective dynamics in a crown fire using infrared video camera imagery. *J Appl Meteorol* 38(10): 1401–1420.
31. Clark TL, Reeder MJ, Griffiths M, Packham D, Krusel N (2005) Infrared observations and numerical modelling of grassland fires in the Northern Territory, Australia. *Meteorol Atmos Phys* 88(3-4):193–201.
32. Canfield JM, Linn RR, Sauer JA, Finney M, Forthofer J (2014) A numerical investigation of interplay between fire line length, geometry, and spread rate. *Agric For Meteorol* 189-190:48–49.
33. Haines DA, Smith MC (1983) Wind tunnel generation of horizontal roll vortices over a differentially heated surface. *Nature* 306:351–352.
34. Patel VC, Sotiropolous F (1997) Longitudinal curvature effects in turbulent boundary layers. *Prog Aerosp Sci* 33:1–70.
35. Floryan JM (1991) On the Görtler instability of boundary layers. *Prog Aerosp Sci* 28:235–271.
36. Li F, Malik MR (1995) Fundamental and subharmonic secondary instabilities of Görtler vortices. *J Fluid Mech* 297:77–100.
37. Lamorlette A (2014) Quantification of ignition time uncertainty based on the classical ignition theory and Fourier analysis. *C R Mec* 342(8):459–465.
38. Wallace J (2013) Highlights from 50 years of turbulent boundary layer research. *J Turbul* 13(53):1–70.
39. Robinson S (1991) Coherent motions in the turbulent boundary layer. *Annu Rev Fluid Mech* 23:601–639.
40. Blackwelder RF, Kaplan RE (1976) On the wall structure of the turbulent boundary layer. *J Fluid Mech* 76(1):89–112.
41. Hamins A, Yang JC, Kashiwagi T (1992) An experimental investigation of the pulsation frequency of flames. *Intl Symp Combust* 24(1):1695–1702.
42. Cetegen B, Ahmed T (1993) Experiments on the periodic instability of buoyant plumes and pool fires. *Combust Flame* 93(1):157–184.
43. Malalasekera WMG, Versteeg HK, Gilchrist K (1996) A review of research and an experimental study on the pulsation of buoyant diffusion flames and pool fires. *Fire Mater* 20(6):261–271.
44. Byram GM (1959) Combustion of forest fuels. *Forest Fire: Control and Use*, ed Davis KP (McGraw-Hill Book Co., New York), Chap 3.
45. Quintiere JG (2006) *Fundamentals of Fire Phenomena* (John Wiley & Sons, New York).
46. Cetegen B, Kasper KD (1996) Experiments on the oscillatory behavior of buoyant plumes of helium and helium-air mixtures. *Phys Fluids* 8(11):2974–2984.
47. Cetegen B, Dong Y, Soteriou MC (1998) Experiments on stability and oscillation behavior of planar buoyant plumes. *Phys Fluids* 10(7):1658–1665.
48. Byram GM, Nelson RM (1974) Buoyancy characteristics of a fire heat source. *Fire Technol* 10(1):68–79.
49. Coen JL, Mahalingam S, Daily JW (2004) Infrared imagery of crown-fire dynamics during FROSTFIRE. *J Appl Meteorol* 43(9):1241–1259.
50. Nelson RM, Adkins CW (1988) A dimensionless correlation for the spread of wind-driven fires. *Can J For Res* 18(4):391–397.
51. Taylor SW, Wotton BM, Alexander ME, Dalrymple GN (2004) Variation in wind and crown fire behaviour in a northern jack pine–black spruce forest. *Can J For Res* 34(8): 1561–1576.
52. Overholt KJ, Cabrera J, Koopersmith M, Ezekoye OA (2014) Characterization of fuel properties and fire spread rates for Little Bluestem grass. *Fire Technol* 50(1):9–38.
53. De Mestre NJ, Catchpole EA, Anderson DH, Rothermel RC (1989) Uniform propagation of a planar fire front without wind. *Comb Sci Technol* 65:231–244.
54. Albini FA (1982) Response of free burning fires to nonsteady wind. *Comb Sci Technol* 29(3-6):225–241.
55. Linn RR, et al. (2012) Using periodic line fires to gain a new perspective on multi-dimensional aspects of forward fire spread. *Agric For Meteorol* 157:60–76.
56. Babrauskas V (2006) Effective heat of combustion for flaming combustion of conifers. *Can J For Res* 36(3):659–663.
57. Babrauskas V (2002) Ignition of wood: A review of the state of the art. *J Fire Prot Eng* 12(3):163–189.
58. Emori RI, Saito K (1983) A study of scaling laws in pool and crib fires. *Comb Sci Technol* 31(5-6):217–230.
59. Adam BA, Akafuah NK, Finney MA, Forthofer J, Saito K (2014) *A Study of Flame Spread in Engineered Cardboard Fuelbeds. Part II: Scaling Law Approach, Progress in Scale Modeling* (Springer, Berlin/Heidelberg, Germany), Vol II, pp 85–95.
60. Wang H, Kläser A, Schmid C, Liu CL (2013) Dense trajectories and motion boundary descriptors for action recognition. *Int J Comput Vis* 103(1):60–79.

Supporting Information

Finney et al. 10.1073/pnas.1504498112

Table S1. Range of experimental variables used in 59 wind tunnel experiments on fire spread through laser-cut cardboard fuel

	Minimum	Maximum
Fuel bed depth (m)	0.025	0.356
Particle width (m)	0.001	0.013
Particle surface area to volume ratio ($m^2 \cdot m^{-3}$)	1,590	3,818
Row spacing (m)	0.0064	0.1572
Packing ratio (ρ_b/ρ_p)*	0.001334	0.088
Fuel loading w ($kg \cdot m^{-2}$)	0.079	2.682
Wind speed ($m \cdot s^{-1}$)	0.11	2.24
Residence time (s)	2	35
Flame depth (m)	0.1	1.2
Flame length observed (m)	0.1	2.5
Fireline intensity (44), $I = hwR$ ($kW \cdot m^{-1}$)*	54	1,728
Flame length (calculated from fireline intensity) (m)	0.49	2.39
Spread rate R ($m \cdot min^{-1}$)	0.57	7.72

*ρ_b bulk density = loading/depth, ρ_p = particle mass density, h = heat content for gas-phase combustion (14 $MJ \cdot kg^{-1}$).

Movie S1. Composite movie of experimental fires burning engineered cardboard fuel beds in the MFSL wind tunnel showing three principal flame dynamics: (*i*) movement of concave flame parcels forward through the flame zone, (*ii*) peak and trough flame structure produced by Taylor-Görtler vorticity, and (*iii*) forward bursting of flames into fresh fuels ahead of the fire.

Movie S1

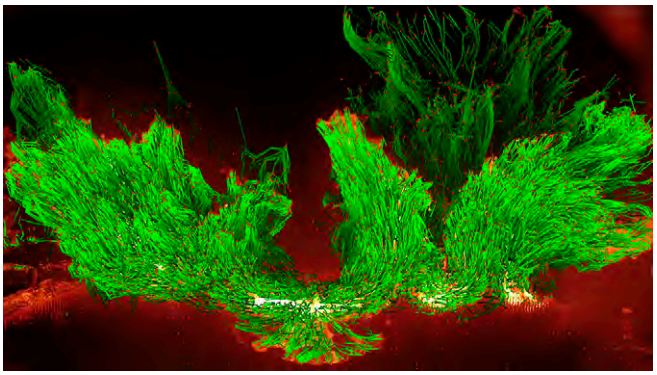

Movie S2. Flow-tracking analysis was used to trace movements of flame parcels in low-speed movie to reveal forward bursting and vorticity patterns of flame peaks and troughs at the leading edge of advancing experimental fire.

Movie S2

Movie S3. Low-speed movie of experimental burn in cardboard fuels uses smoke to visualize vorticity of the airflow behind the approaching flame zone.

Movie S3

Movie S4. Close-up view from high-speed movie shows forward flame bursts and peak and trough flame structure at the leading edge of an approaching fire in the MFSL wind tunnel burning engineered cardboard fuel bed.

Movie S4

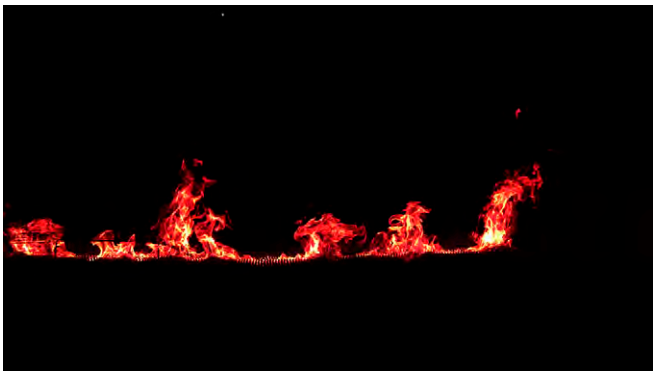

Movie S5. Wide-angle view from high-speed movie shows peak and trough structure of 0.2-m flames at the leading edge of an approaching fire in the MFSL wind tunnel burning engineered cardboard fuel bed.

Movie S5

Movie S6. Movie of prescribed fire in 1-m tall grass at Camp Swift, Texas, showing peak and trough structure of approaching flames (~3 m tall) and position of thermocouple rakes wrapped in aluminum foil (left).

Movie S6